Available online at www.sciencedirect.com
ScienceDirect
Chemical Physics 341 (2007) 344–356
Chemical Physics
www.elsevier.com/locate/chemphys

Polarizability response spectroscopy: Formalism and simulation of ultrafast dynamics in solvation

Andrew M. Moran *, Sungnam Park [1], Norbert F. Scherer

Department of Chemistry and the James Franck Institute, The University of Chicago, 929 East 57th Street, Chicago, IL 60637, USA

Received 22 February 2007; accepted 5 September 2007
Available online 11 September 2007

Abstract

A formalism is presented for a novel fifth-order spectroscopy designed to measure the spectrum of nuclear modes coupled to photo-induced processes. In this description of polarizability response spectroscopy, a two-level system first interacts (twice) with an electronically resonant laser pulse to create ground and excited state wavepackets that evolve until the polarizability spectrum is probed by three off-resonant pulses and a fourth local oscillator probe field. In the experiment and in the present formalism, heterodyne detection is accomplished by tuning the relative phase of a local oscillator field with respect to the signal field. Full field-resolved signal detection by spectral interferometry is also described with the formalism of this paper. Terms in the response function involving electronic ground and excited state populations are shown to be 180 degrees out-of-phase. We present a model for which signal generation in the presence of these interfering terms results from two mechanisms: structural relaxation induced resonance and dephasing-induced resonance. Our model shows that interference between ground and excited state terms in the PORS response function may be interpreted as arising from the overlap of hole and particle nuclear wavepackets in coordinate space. These results are discussed in the context of experimental measurements for Coumarin 153-Solvent systems. Comparison of theoretical and experimental signals suggests that structural relaxation-induced resonance of the solvent is the primary origin of the measured signals in both solvation and charge transfer processes.
© 2007 Elsevier B.V. All rights reserved.

Keywords: Nonlinear spectroscopy; Solvent dynamics; Solvation

1. Introduction

Condensed phase chemical reactions are mediated by interactions with the solvent surroundings. Solvent motions (fluctuations) provide the energy needed for reactants to surmount potential energy barriers and serve as a bath for energy dissipation after product formation. For example, solvents with large dielectric constants reduce the free energy barrier for charge and proton transfer reactions [1–3]. Thus, reactive channels exist between states in solution that do not couple in the gas phase. Nuclear modes vibrate and fluctuate on the femtosecond time-scale. For this reason, a variety of ultrafast laser spectroscopies have been developed to study solvent dynamics. Time-resolved fluorescence Stokes shift [4–8] and pump–probe techniques [9–11] follow nonequilibrium relaxation (i.e., solvation) of a solute following photoexcitation. In contrast, photon-echo experiments are sensitive to equilibrium fluctuations of a solute's transition energy [12–16]. Information on solvation dynamics is restricted to the framework of linear response for these third-order spectroscopies, where solute–solvent interactions are fully described by two-time correlation functions [17,18]. Therefore, these methods do not yield the evolution of solute–solvent interactions with nonequilibrium relaxation (i.e., the instantaneous spectral density). Higher-order spectroscopies are needed to uncover the three-point correlation functions containing this information [18–23].

* Corresponding author. Present address: Department of Chemistry, The University of North Carolina, Chapel Hill, NC 27599, USA.
E-mail address: ammoran@email.unc.edu (A.M. Moran).
[1] Present address: Department of Chemistry, Stanford University, Stanford, CA 94305, USA.

0301-0104/$ - see front matter © 2007 Elsevier B.V. All rights reserved.
doi:10.1016/j.chemphys.2007.09.001

Two recently developed laser spectroscopies are designed to measure the spectrum of low frequency solvent motion coupled to nonequilibrium reactive processes in condensed phases. Polarizability response spectroscopy (PORS) [24–27] and resonant pump third-order Raman spectroscopy (RaPTORS) [21,28,29] differ in implementation but seek to measure the same dynamics. For example, dipolar solvation has been investigated with both methods [21,24,25]. More recently, solvent dynamics induced by an intramolecular proton transfer [29] and intermolecular charge transfer [26,27] reactions have been studied. These data suggest that both methods are successful in probing nonequilibrium solvent dynamics driven by photoinitiated events. However, these previous experiments (except those in Refs. [26,27]) were interpreted using models that do not account for all aspects of the observed signals. Most notably, the sign of the signal has been found to depend on the chemical system and the temporal delays of the laser pulses. Here we show that interference between terms in the fifth-order nonlinear response function may give rise to both positive and negative signals.

The present theoretical paper is a complement to our experimental elaboration of PORS in which solvation of Coumarin 153 (C153) is investigated in various solvents [25,30]. These experiments involve one-dimensional measurements in which the polarizability spectrum of the solvent is probed at a single delay time after solvation is complete or as two-dimensional measurements that monitor evolution of the polarizability spectrum during the solvation process. This formalism has also been applied to a recent PORS study of solvent response to intermolecular charge transfer, where the rate formula is parameterized with the experimental PORS signals to quantify the effect of solvation dynamics on the observed kinetics [26,27].

We describe the PORS experiment as a sequential process in which the electronic excitation of a solute with the resonant laser pulse precedes an off-resonant Raman probe of the resulting nuclear dynamics. The expressions in the present paper are motivated by the doorway–window formalism originally applied to third-order pump–probe spectroscopy [31]. This formalism is well-suited to describing nonlinear spectroscopies, such as PORS, in which population dynamics are of interest (in contrast to photon-echo methods that probe optical coherences) and produces realistic signals because delta function laser pulses are not assumed. Approximations intrinsic to this intuitive view of the experiment are defined and important terms in the material response function are identified. Knowledge of the dominant terms and their respective phases is critical for understanding the experimentally observed signs of the signals. Similar interference effects were observed in coherent Raman spectroscopies in the early 1980s [32–34], and were recently predicted for second-order difference frequency mixing experiments [35], which further emphasizes the importance of understanding the various contributions to the PORS signal. To obtain further physical insight, we show that terms with opposite signs may be represented by hole and particle wavepackets. In this semiclassical representation, the amount of interference between competing terms in the PORS response function is mapped on to the overlap of these nuclear wavepackets in coordinate space.

The general approach taken here may be useful for interpreting related fifth-order spectroscopies. For example, Mathies and co-workers have developed the technique of Femtosecond Stimulated Raman spectroscopy (FSRS) [36], which was recently applied to the isomerization of rhodopsin to obtain sub-100 fs time-resolved vibrational spectra that cover the entire fingerprint region [37]. FSRS is similar to PORS in that the experiment can be viewed as a sequence of two events: electronic excitation of a chromophore followed by a Raman probe of nuclear dynamics. The two methods differ in that PORS intentionally enhances the solvent response by requiring the Raman probe to be off-resonant with respect to electronic transitions of the solute, whereas FSRS has sought to measure intramolecular vibrations of solutes. A key finding of this paper is that all fifth-order experiments using this general pulse sequence measure polarization responses associated with the ground and excited states of the solute that are 180° out-of-phase.

General equations for fifth-order nonlinear spectroscopy are given in the next section. In Section 3, a formal expression for the sequential PORS signal is derived and model calculations are presented. The 16 terms in the PORS response function (i.e., Liouville space pathways) are discussed in Section 4. We conclude in Section 5 and discuss future directions.

2. Fifth-order nonlinear spectroscopy

Under perfect phase matching conditions, a frequency component of the fifth-order polarization, $P^{(5)}(\omega_t)$, is related to the emitted signal field by

$$E^{(5)}(\omega_t) = \frac{i2\pi l\omega_t}{n(\omega_t)c} P^{(5)}(\omega_t), \tag{1}$$

where $n(\omega_t)$ is the sample's refractive index, l is the sample length, c is the speed of light and t_i represent time intervals between the six field-matter interactions (Fig. 1a). In general, $P^{(5)}(\omega_t)$ is expressed as a convolution of the fifth-order nonlinear response function $R^{(5)}(t_5,t_4,t_3,t_2,t_1)$ with five laser pulses $E_i(t-t_5\cdots)$:

$$\begin{aligned} P^{(5)}(t) = \int_0^\infty dt \int_0^\infty dt_5 \int_0^\infty dt_4 \int_0^\infty dt_3 \int_0^\infty dt_2 \int_0^\infty \\ \times dt_1 R^{(5)}(t_5,t_4,t_3,t_2,t_1) E_5(t-t_5) E_4(t-t_5-t_4) \\ \times E_3(t-t_5-t_4-t_3) E_2(t-t_5-t_4-t_3-t_2) \\ \times E_1(t-t_5-t_4-t_3-t_2-t_1). \end{aligned} \tag{2}$$

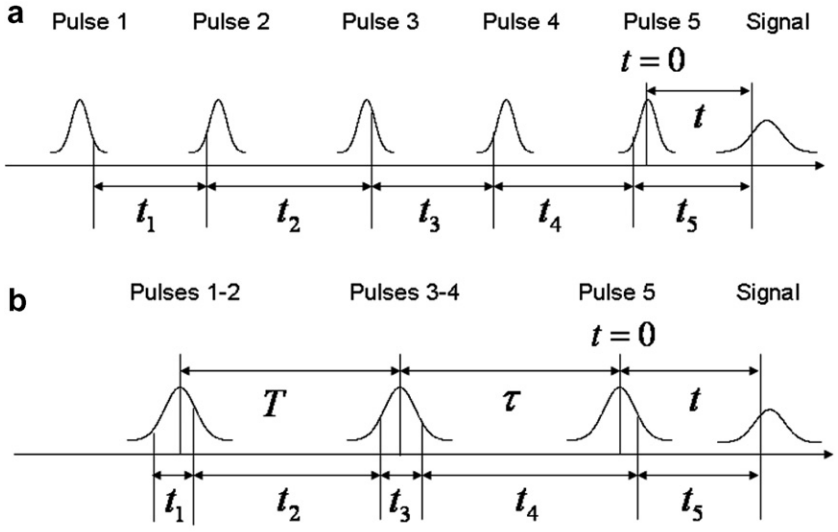

Fig. 1. Time variables represent the (a) general formulation of fifth-order nonlinear spectroscopy and (b) those defined to describe PORS as a sequential process. In panel (b), T is the experimentally controlled delay between the E_1&E_2 and E_3&E_4 pulse pairs; τ is the experimentally controlled delay between pulses 3&4 and pulse 5.

The fifth-order response function may be written as

$$R^{(5)}(t_5,t_4,t_3,t_2,t_1) = \left(\frac{-\mathrm{i}}{\hbar}\right)^5 \langle V|\mathscr{G}(t_5)\mathscr{V}\mathscr{G}(t_4)\mathscr{V}\mathscr{G}(t_3) \times \mathscr{V}\mathscr{G}(t_2)\mathscr{V}\mathscr{G}(t_1)\mathscr{V}|\rho_{\mathrm{eq}}\rangle, \quad (3)$$

where ρ_{eq} is the equilibrium density operator. The Liouville space Green function, $\mathscr{G}(t)$, and dipole operator, $\mathscr{V}$, are defined by

$$\mathscr{G}(t)\rho(0) = \exp(-\mathrm{i}Ht/\hbar)\rho(0)\exp(\mathrm{i}Ht/\hbar) = \rho(t) \quad (4)$$

and

$$\mathscr{V}\rho = [V,\rho], \quad (5)$$

where V is the Hilbert space molecular dipole operator [18]. There are 64 terms in $R^{(5)}(t_5,t_4,t_3,t_2,t_1)$ assuming temporally separated delta function pulses. This number increases by 5! when permutations of the electric fields are considered. The PORS response function is defined by a small subset of these terms. In the following sections, we introduce approximations and show how the PORS laser pulse configuration suppresses contributions from undesired terms.

3. PORS as a sequential process

3.1. PORS pulse configuration

The electric field for a sequence of six laser pulses may be written as

$$E(\mathbf{r},t) = \sum_{n=1}^{6}[E_n(\mathbf{k}_n,t) + E_n^*(\mathbf{k}_n,t)], \quad (6)$$

where

$$E_n(\mathbf{k}_n,t) = \epsilon_n(t-\bar{\tau}_n)\exp[\mathrm{i}\mathbf{k}_n\mathbf{r} - \mathrm{i}\bar{\omega}_n t - \mathrm{i}\phi_n(t)]. \quad (7)$$

In Eq. (7), $\epsilon_n(t-\bar{\tau}_n)$ is a slowly varying envelope function for pulse n centered at time $\bar{\tau}_n$ with carrier frequency $\bar{\omega}_n$, wavevector $\mathbf{k}_n$, and the temporal phase function $\phi_n(t)$. The experiment involves five incident laser pulses and the sixth is used for heterodyne detection of the signal field, $E_{\mathrm{LO}}(\mathbf{k}_{\mathrm{LO}},t) = E_6(\mathbf{k}_6,t)$. Transform limited pulses are used in our experimental work [24–27], so $\phi_n(t)$ are taken to be time-independent for pulse n and will be denoted as ϕ_n^0. The experimentally controlled pulse delays are defined as $\bar{\tau}_1 = \bar{\tau}_2 = T+\tau$, $\bar{\tau}_3 = \bar{\tau}_4 = \tau$ and $\bar{\tau}_5 = 0$ [25,30].

In the sequential view of PORS, the system first interacts with the electronically *resonant* fields (E_1 and E_2) before the *off-resonant* fields (E_3, E_4 and E_5). Furthermore, the two field-matter interactions associated with the E_3&E_4 field pair precede the interaction with E_5. All five laser pulses are off-resonant with respect to solvent (electronic) transitions. This sequence of field-matter interactions and the experimentally controlled pulse arrival times are illustrated in Fig. 1b. We note that a single resonant pulse, E_{RP}, is used in our experimental implementations [24–27].

With the external electric field and pulse delays defined above, the fifth-order source of the PORS signal field is given by

$$P^{(5)}_{\mathrm{PORS}}(\mathbf{k}_s,t,\tau,T) = \int_0^\infty \mathrm{d}t_5 \int_0^\infty \mathrm{d}t_4 \int_0^\infty \mathrm{d}t_3 \int_0^\infty \mathrm{d}t_2 \times \int_0^\infty \mathrm{d}t_1 R^{(5)}(t_5,t_4,t_3,t_2,t_1) E_5(\mathbf{k_5}, t - t_5) E_4(\mathbf{k_4}, t+\tau-t_5-t_4) E_3^*(\mathbf{k_3}, t+\tau-t_5-t_4-t_3) E_2(\mathbf{k_2}, t+\tau+T-t_5-t_4-t_3-t_2) E_1^*(\mathbf{k_1}, t+\tau+T-t_5-t_4-t_3-t_2-t_1), \quad (8)$$

where $\mathbf{k_s} = -\mathbf{k_1}+\mathbf{k_2}-\mathbf{k_3}+\mathbf{k_4}+\mathbf{k_5}$. Eq. (8) is no less cumbersome to evaluate than Eq. (2). To derive a more

tractable formula, the number of nested integrals in Eq. (8) must be reduced by applying the approximations outlined in the next section.

3.2. Approximations

As suggested above, the PORS experiment is most naturally viewed as a sequential process in which the system interacts with a resonant laser pulse ($E_{RP} = E_1 + E_2$) to populate its electronic ground and excited states, evolves freely according to the respective electronic state Hamiltonian and is then interrogated by an off-resonant Raman probe (E_3, E_4 and E_5). This is formally accomplished by introducing five approximations: (i) the durations of the pulses are short compared to the experimentally controlled delays T and τ; (ii) the dephasing time intervals t_3 and t_5 for the off-resonant interactions are much shorter than the pulse duration and may be removed from the electric field arguments; (iii) the pulses are short compared to nuclear dynamics; (iv) the wavelength dependence of the off-resonant Raman scattering cross section during t_3 and t_5 is sufficiently weak that the actual frequencies may be approximated by the average of the two frequencies intrinsic to the Raman scattering process; (v) the rotating wave approximation.

3.3. Nonequilibrium polarizability susceptibility

In this section, $R^{(5)}(t_5,t_4,t_3,t_2,t_1)$ is rewritten as a nonequilibrium correlation function that consists of three nuclear wavepackets. The doorway wavepacket prepared by the first two field-matter interactions is given by

$$D(\omega_1) \equiv \int_{-\infty}^{\infty} d\omega_1' I(\omega_1' - \omega_1) \int_0^{\infty} dt_1 [\mathscr{V}\mathscr{G}(t_1)\mathscr{V}\rho_{eq}] \times \exp(i\omega_1' t_1), \tag{9}$$

where $I(\omega_1' - \omega_1)$ is the power spectrum of pulses 1 and 2. Eq. (9) is the convolution of $I(\omega_1' - \omega_1)$ with Mukamel's snapshot doorway wavepacket and represents the case where pulses 1 and 2 are short compared to nuclear dynamics [approx. (iii)] but not compared to optical dephasing [18]. The polarizability operator intrinsic to the final four field-matter interactions is defined as [18]

$$\alpha(\omega_{pr}) \equiv \int_0^{\infty} dt [\mathscr{V}\mathscr{G}(t)\mathscr{V}] \exp(i\omega_{pr} t) - \text{h.c.} \tag{10}$$

where $\omega_{pr} = (\omega_3 + \omega_5)/2$ [approx. (iv)]. The frequency dependence of $\alpha(\omega_{pr})$ is very weak in our experiments where the solutions are transparent at ω_{pr} [24–27]. We hereafter suppress this argument.

The material response function can now be rewritten in terms of these wavepackets. It is important to note that as a consequence of Eq. (9) the resulting correlation function depends on the spectrum of the resonant $E_1\&E_2$ pulse pair whereas $R^{(5)}(t_5,t_4,t_3,t_2,t_1)$ is a purely material function. The present approach is useful as it allows subsequent manipulations to be carried out on the same footing as those for the third-order polarizability susceptibility. The nonequilibrium PORS correlation function is then written as

$$\Phi_{PORS}(t_4, T, \omega_1) = \frac{i|\mu_{eg}|^2}{\hbar^5} \langle [\alpha(0), \alpha(t_4)] D(T, \omega_1) \rangle, \tag{11}$$

where Eq. (4) is used to write $D(\omega_1)$ and α as time-dependent operators and we have assumed that $t_2 \approx T$ [approx. (i)]. Eq. (11) resembles the third-order coherent Raman scattering response function under similar approximations. The polarizability susceptibility is given by [31]

$$\chi(t) = \frac{-i}{\hbar} \langle [\alpha(t), \alpha(0)] \rho_{eq} \rangle. \tag{12}$$

The fundamental difference between Eqs. (11) and (12) is that the polarizabilities are projected onto the equilibrium density operator in Eq. (12), whereas they are projected onto the nonequilibrium doorway wavepacket in Eq. (11).

3.4. PORS source polarization

With the results of the previous section, the fifth-order source polarization for the PORS signal field is written as

$$P^{(5)}_{PORS}(t,\tau,T,\omega_1) = \frac{-iE_5(t)|\mu_{eg}|^2}{\hbar^5} \int_0^{\infty} dt_4 \langle [\alpha(0), \alpha(t_4)] D(T, \omega_1) \rangle \times E_4(t + \tau - t_4) E_3^*(t + \tau - t_4). \tag{13}$$

Eq. (13) is analogous to the third-order polarization for coherent Raman scattering under similar approximations. It should be emphasized that since the $E_1\&E_2$ pulse pair is well-separated from the $E_3\&E_4$ pulse pair [approx. (i)] the upper limit for t_4 in Eq. (13) may be infinite without violating the assumption of a sequential process. It is important to keep t_4 as an integration variable when high-frequency modes (compared to the bandwidths of pulses 3–5) contribute to the PORS signals [38]. However, pulses 3–5 may be taken to be delta functions in time when their bandwidths are large compared to the mode frequencies of the material polarizability spectrum. In this limit, Eq. (13) becomes

$$P^{(5)}_{PORS}(t,\tau,T,\omega_1) = \frac{-i|\mu_{eg}|^2}{\hbar^5} \langle [\alpha(0), \alpha(\tau)] D(T, \omega_1) \rangle. \tag{14}$$

Finally, Eq. (1) is used to write the PORS signal field

$$E^{(5)}_{PORS}(t,\tau,T) = \frac{i2\pi l \bar{\omega}_t}{n(\bar{\omega}_t)c} P^{(5)}_{PORS}(t,\tau,T), \tag{15}$$

where $\bar{\omega}_t$ is the carrier frequency of the PORS signal pulse and the dependence on the $E_1\&E_2$ carrier frequency, ω_1, has been suppressed. Eq. (15) assumes that the refractive index of the sample is constant over the bandwidth of the signal. The dispersive part of $E^{(5)}_{PORS}(t,\tau,T)$ is selectively measured experimentally using the heterodyne detection method described in Appendix A [25,30]. We note that our newly developed apparatus provides the full signal

field, $E^{(5)}_{\mathrm{PORS}}(t,\tau,T)$, through detection by spectral interferometry [26,27].

Eq. (13) differs from that found under the assumption of impulsive pulses in two important ways. First, the effect of the spectrum of the resonant pulse ($E_{\mathrm{RP}} = E_1 + E_2$) on nonequilibrium dynamics of $D(T,\omega_1)$ in T is incorporated with the convolution in Eq. (9). In the following section, we discuss the sensitivity of the PORS signal to the dynamics of $D(T,\omega_1)$. Second, it captures spectral filtering effects for modes in the polarizability [38]. Pulses 3–5 are assumed to be impulsive in Eq. (14) and therefore this expression yields a realistic signal only when the pulses 3–5 are short compared to nuclear dynamics in τ [approx. (iii)].

3.5. Model calculations

Results given above are illustrated in this section with numerical calculations of PORS signals. The model consists of two electronic states and three harmonic solvent modes, which have equal ground and excited state frequencies but displaced potential minima. The parameters for a single mode are defined in Fig. 2. The present analytical model offers important physical insight by clearly defining the two primary mechanisms of signal generation. Molecular dynamics simulations will be needed to provide a more complete microscopic picture of the nuclear motions that underly the PORS signals from actual samples.

Closed expressions for propagation of $D(\omega_1)$ (Eq. (9)) in T were previously presented in the limit of static line broadening with an overdamped Brownian oscillator bath [18]. Overdamped nuclear motion is an appropriate description because recurrences are not observed in the experiments during the T interval [25,30]. In dimensionless units, the center frequencies of the hole and particle are

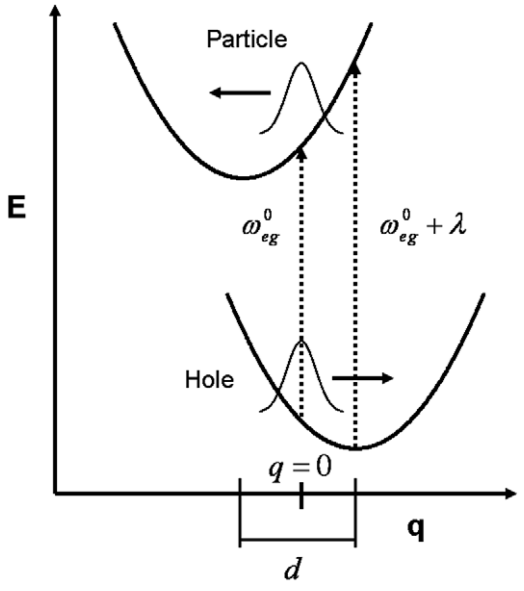

Fig. 2. A harmonic mode with displaced ground and excited state potential minima. The mode-specific reorganization energy is given by $\lambda_j = \frac{1}{2}\omega_j d_j^2$ with the dimensionless displacement d_j and mode frequency ω_j.

$$q^g_j(T) = \frac{\lambda_j + M_j(T)[(\omega_0 - \omega^0_{\mathrm{eg}}) - \lambda_j]}{\omega_j d_j} \tag{16a}$$

and

$$q^e_j(T) = \frac{-\lambda_j + M_j(T)[(\omega_0 - \omega^0_{\mathrm{eg}}) + \lambda_j]}{\omega_j d_j}, \tag{16b}$$

where

$$\omega_0 = \frac{2\lambda_j\omega_{1,2}}{2\lambda_j + \beta\delta\omega^2_{1,2}} + (\omega^0_{\mathrm{eg}} + \lambda_j)\frac{\delta\omega^2_{1,2}}{2\lambda_j + \delta\omega^2_{1,2}}. \tag{16c}$$

Here j is the index for nuclear modes, m represents the electronic state, ω^0_{eg} is the electronic transition frequency, $M(T)$ is the solvation correlation function, $\delta\omega_1$ is the bandwidth of the $E_1\&E_2$ pulse pair and λ_j is the reorganization energy of mode j. The time-dependent widths of the hole and particle are given by

$$\delta q^2_j(T) = \frac{\Delta^2_j}{d^2_j\omega^2_j}\left[1 - \frac{\Delta^2_j}{\Delta^2_j + \delta\omega^2_1}M^2_j(T)\right]. \tag{17}$$

Eq. (17) shows that the wavepacket does not assume its asymptotic width immediately upon excitation due to the finite spectral bandwidth of the $E_1\&E_2$ pulse pair. With Eqs. (16)–(17), the doorway wavepacket for mode j on the potential energy surface of state m may be written as

$$D^m_j(q_j,T) = \frac{1}{\delta q_j(T)\sqrt{2\pi}}\exp\left[\frac{(q_j - q^m_j(T))^2}{2\delta q^2_j(T)}\right]. \tag{18}$$

This result represents propagation of Eq. (9) with $\mathcal{G}(T)$ (see Eq. (4)).

A working form of Eq. (14) can now be found by expressing the PORS source polarization as

$$P^{(5)}_{\mathrm{PORS}}(\tau,T) = \sum_j \frac{\mathrm{i}|\mu_{\mathrm{eg}}|^2}{\hbar^5}\langle[\alpha_j(q_j),\alpha_j(q_j,\tau)]\{D^g_j(q_j,T) - D^e_j(q_j,T)\}\rangle\exp(-\mathrm{i}\omega_j\tau) \tag{19}$$

in a basis of discrete nuclear modes j. Homogeneous dephasing is assumed during τ to minimize the number of parameters. Furthermore, we consider only excitations at the fundamental mode frequencies. In these approximations, Eq. (19) becomes

$$P^{(5)}_{\mathrm{PORS}}(\tau,T) = \sum_j \Phi^g_j(\tau,T) - \Phi^e_j(\tau,T), \tag{20a}$$

where

$$\Phi^m_j(\tau,T) = \frac{\mathrm{i}|\mu_{\mathrm{eg}}|^2}{\hbar^5}\left[1 - \exp\left(-\frac{\hbar\omega_j}{kT}\right)\right]\exp[\mathrm{i}\omega_j\tau - \Gamma^m_j\tau] \times \int_{-\infty}^{\infty} \mathrm{d}q_j|\alpha_j(q_j)|^2 D^m_j(q_j,T). \tag{20b}$$

In Appendix B, we show how the approximation of linear response is used to write Eq. (20). Eq. (20) shows that the PORS signal vanishes when $\Phi^g_j(\tau,T) = \Phi^e_j(\tau,T)$. *The differences in $\Phi^g_j(\tau,T)$ and $\Phi^e_j(\tau,T)$ yield the two primary mecha-*

nisms of PORS signal generation: (*i*) *structural relaxation-induced resonances occur as a result of the coordinate dependence of the polarizability*, $\alpha_j(q_j)$; (*ii*) *dephasing-induced signal generation occurs when* $\Gamma_j^g \neq \Gamma_j^e$.

The parameters used for numerical evaluation of (20) are summarized in Table 1. Our goal is not to fit the experimental data, but rather to gain physical insight by assuming a realistic set of parameters and computing signals. The frequencies of the three modes are 5, 10 and 50 cm^{-1}. In Ref. [39], these three "mode" frequencies were taken to represent diffusive reorientation, interaction-induced and librational solvent motions [39,40]. Interaction-induced motion is translational whereas diffusive reorientation and libration describe individual molecule and collective reorientational motion, respectively. The dephasing rates, Γ_j^m, for all three modes in the ground and excited states are assumed to be 0.005 fs^{-1}. The coordinate-dependent polarizabilities are taken to be independent of the electronic state of the solute. The first derivative of the coordinate-dependent polarizabilities for all three modes is given by $\alpha_j'(q_j) = 1.0 - 0.01q_j$ (see Appendix B). This is not an obvious choice. However, it is merely important that the first derivative of the polarizability possesses nonzero coordinate-dependence to illustrate the two signal generation mechanisms. Furthermore, by assuming the slope of $\alpha_j'(q_j)$ to be negative the polarizabilities increase upon excitation, which is a known property of C153 in solution [41–43]. The duration of the $E_1\&E_2$ pulse pair is assumed to be 50 fs.

The PORS signal, $\mathrm{Re}\{E_{\mathrm{PORS}}^{(5)}(\tau, T)\}$, presented in Fig. 3 is computed using Eqs. (15) and (20). Both the calculated and experimental signals rise to the maximum value within the first few picoseconds in T [25,30]. However, the measured signal decays more slowly along the τ-axis as T increases [25,30]. Eq. (20) cannot account for this with its current assumptions. However, the T-dependence of the dephasing rates, Γ_j^m, may be introduced in our model by allowing the dephasing rates to be coordinate dependent. Thus, the experimental results suggest that the dephasing rates for the nuclear modes associated with the PORS signal depend on the structure of the Coumarin 153-acetonitrile system, hence the approximation of linear response does not hold for this system (see Appendix B).

Table 1
Summary of model parameters

Parameters[a]	Value
ω_1	5 cm^{-1}
ω_2	10 cm^{-1}
ω_3	50 cm^{-1}
λ_j	500 cm^{-1}
Γ_j^g	0.005 fs^{-1}
Γ_j^e	0.005 fs^{-1}
$\alpha_j'(q_j)$[b]	$1.0 - 0.01q_j$

[a] Parameters are defined in Eq. (20). The subscript j denotes all three modes. The solvation correlation function for all three modes is given by $M_j(T) = 0.686\exp(-T/0.089) + 0.314\exp(-T/0.63)$ [41].
[b] See Appendix B.

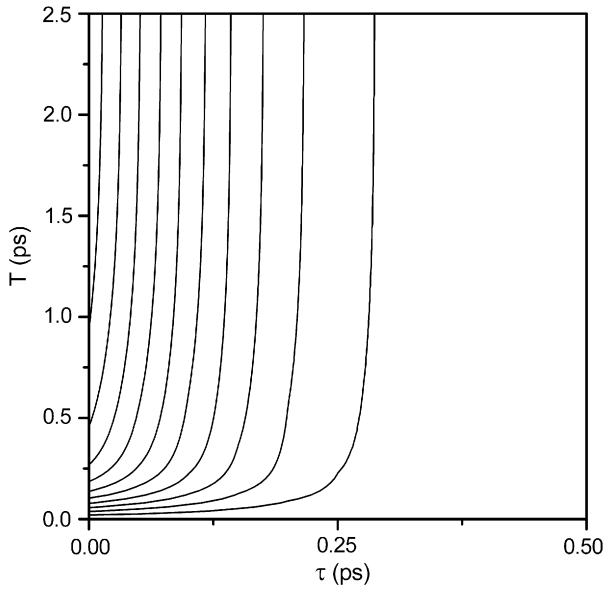

Fig. 3. Dispersive PORS signal, $\mathrm{Re}\{E_{\mathrm{PORS}}^{(5)}(\tau, T)\}$, calculated using Eqs. (15) and (20).

The profile for $\mathrm{Re}\{E_{\mathrm{PORS}}^{(5)}(\tau, T)\}$ at $\tau = 100$ fs is shown in Fig. 4. The shape of the experimental signal profile suggests a relaxation process occurring on the picosecond time-scale that enhances signal generation [25,30]. The agreement

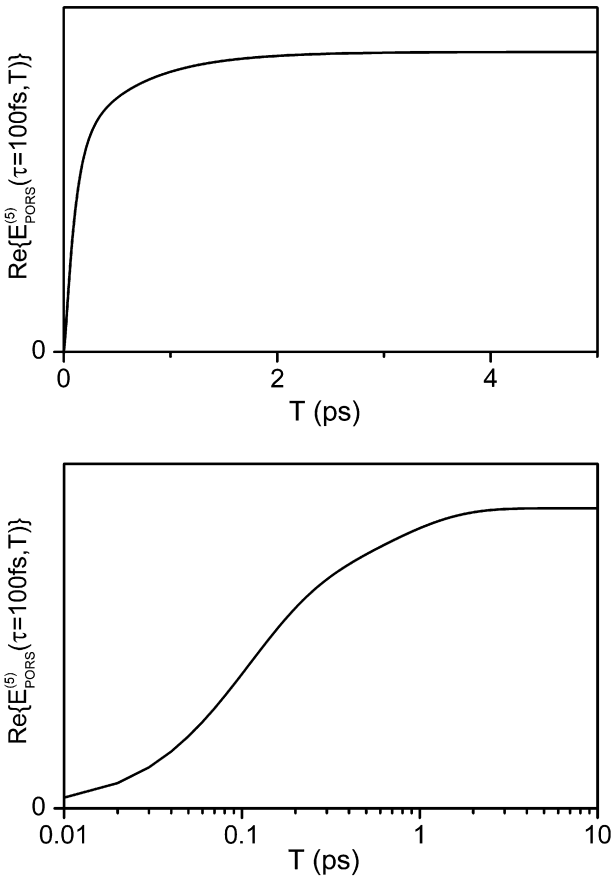

Fig. 4. Dispersive PORS signal, $\mathrm{Re}\{E_{\mathrm{PORS}}^{(5)}(\tau = 0, T)\}$, calculated using Eqs. (15) and (20) plotted on linear (top) and log (bottom) scales.

between Eq. (20) and the experimental signal profile for $T < 2$ ps validates the treatment of the polarizability response in our model. We have taken the coordinate-dependent polarizabilities, $\alpha_j(q_j)$, to be independent of the electronic state of the solute. Therefore, $\Phi_j^g(\tau, T)$ and $\Phi_j^e(\tau, T)$ of Eq. (20) are equivalent at $T = 0$ ps and $P_{\mathrm{PORS}}^{(5)}(\tau, T)$ vanishes. The difference between $\Phi_j^g(\tau, T)$ and $\Phi_j^e(\tau, T)$ increases with T because of nuclear relaxation and the coordinate dependence of the polarizabilities [mechanism (i)]. The alternative choice in writing Eq. (20) is to assume the polarizabilites depend on the electronic state of the solute and change instantaneously upon excitation. However, this treatment is not consistent with the experiment because the calculated PORS signal would then rise as a step function at $T = 0$ ps.

We have denoted structural relaxation-induced resonance as mechanism (i) for PORS signal generation. This mechanism is illustrated in Fig. 5, where the hole and particle wavepackets are presented alongside the corresponding PORS signal at delay time, T. Here we have defined the polarizability spectral density, $\xi(\omega_\tau, T)$, as the imaginary part of the inverse Fourier transform of Eq. (20) with respect to τ:

$$\xi(\omega_\tau, T) = \mathrm{Im}\left[\frac{2\pi l \bar{\omega}_t}{n(\bar{\omega}_t)c} \int_{-\infty}^{\infty} P_{\mathrm{PORS}}^{(5)}(\tau, T = T_{\mathrm{eq}}) \exp(\mathrm{i}\omega\tau)\mathrm{d}\tau\right]. \tag{21}$$

These calculations show that the PORS signal is not emitted at $T = 0$ ps because the hole and particle wavepackets occupy the same range of coordinate space. The magnitude of the signal increases when the hole and particle move to different locations as a result of nuclear relaxation. Thus, nonequilibrium relaxation of the particle and hole wavepackets gives rise to the picosecond rise time of the signal amplitude in Fig. 4.

Dephasing-induced resonance is mechanism (ii) for PORS signal generation. The effects of mechanism (i) are suppressed in the calculation presented in Fig. 6 by taking the reorganization energies of the modes, λ_j, to be zero. That is, the ground and excited state wavepackets are perfectly overlapped in coordinate space at all T. The signals are computed at $T = 4$ ps with ratios $\Gamma_j^g/\Gamma_j^e = 0.97$, 0.99 and 1.00, where $\Gamma_j^e = 0.005\ \mathrm{fs}^{-1}$. We see that in the absence of mechanism (i) no signal is emitted for the ratio $\Gamma_j^g/\Gamma_j^e = 1.00$. However, the signal magnitude increases as this ratio deviates from unity. These line shapes are unlike those presented in Fig. 5 and the experimental spectra [25], which suggests that mechanism (i) is more important than mechanism (ii). These dephasing-induced resonances (the signal vanishes when $\Gamma_j^e = \Gamma_j^g$) are reminiscent of similar observations in picosecond coherent Raman spectroscopies on vapors [32,34] and low-temperature solids [33], where pressure (vapor) or temperature (solid) was found to be

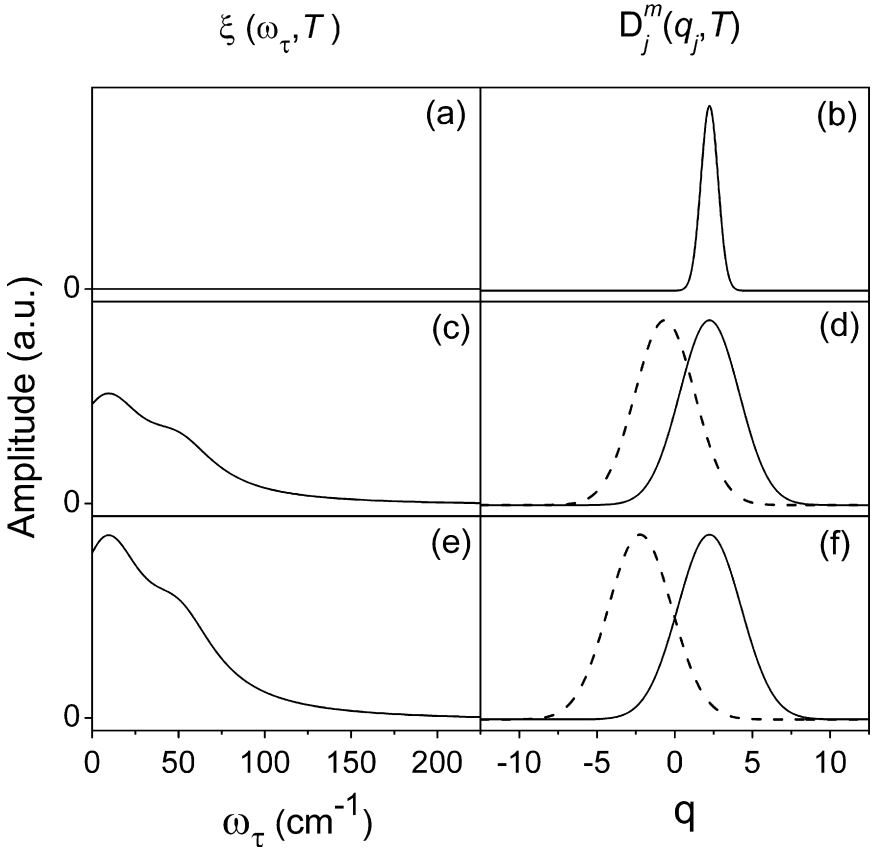

Fig. 5. Illustration of mechanism (i) for PORS signal generation: structural relaxation-induced resonance. The PORS spectra in the left column, $\xi(\omega_\tau, T)$, are calculated with Eq. (21). The hole (solid) and particle (dashed) wavepackets in the right column, $D_j^m(q_j, T)$, are calculated using Eq. (18). Each row represents a single delay time, T. Panels (a)-(b), (c)-(d) and (e)-(f) correspond to delay times T of 0, 0.16 and 4 ps, respectively.

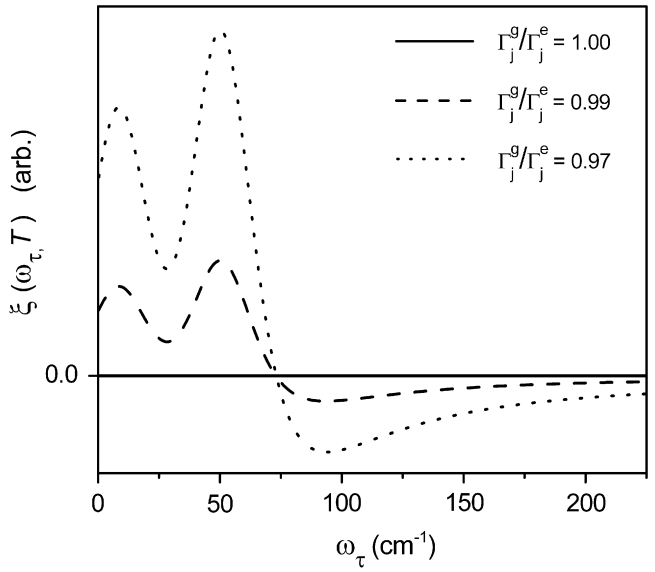

Fig. 6. Illustration of mechanism (ii) for PORS signal generation: dephasing-induced resonance. The polarizability susceptibility, $\xi(\omega_\tau,T)$, is computed at $T = 4$ ps using Eq. (21) with various ratios of Γ_j^g/Γ_j^e. The solid, dashed and dotted lines correspond to ratios, Γ_j^g/Γ_j^e, of 1.00, 0.99 and 0.97, respectively.

correlated with signal strength. Terms associated with the ground and excited states are also 180° out-of-phase in electronically resonant coherent third-order Raman spectroscopies [18].

4. Liouville space pathways

Results presented in the previous section suggest an intuitive interpretation of the PORS signals, but do not reveal the phases of individual terms in $R^{(5)}_{\mathrm{PORS}}(t_5,t_4,t_3,t_2,t_1)$. As discussed above, positive and negative signals may be observed because terms associated with the ground and excited states are 180° out-of-phase. In this section, we present the eight unique (neglecting complex conjugates) Liouville space pathways in $R^{(5)}_{\mathrm{PORS}}(t_5,t_4,t_3,t_2,t_1)$ that are consistent with our five approximations. The terms are expressed using Liouville space generating functions (LGF) [18] because this approach establishes a clear connection to the wavepackets in Section 3. The origin of the phase for each term is well-defined in this representation.

A basis of electronic states must be introduced. The indices g and e represent the ground and excited electronic states of the composite solute–solvent system; the $E_1\&E_2$ pulse pair is resonant with the energy gap between these two states. The indices f and f' correspond to higher-energy electronic states of the system needed to write expressions for the off-resonant interactions. Nuclear substates are not treated explicitly as they are not needed to identify the dominant pathways in the response function.

The second-order LGFs are found by expanding the material part of Eq. (9), $[\mathscr{V}\mathscr{G}(t_1)\mathscr{V}\rho_{\mathrm{eq}}]$, then propagating the system for t_2 on either the ground or excited state potential energy surface. The four resulting LGFs are given by

$$\rho_1(t_1+t_2) = G_{gg}(t_2)V_{ge}G_{\mathrm{eg}}(t_1)V_{\mathrm{eg}}\rho_{\mathrm{eq}}, \tag{22a}$$

$$\rho_2(t_1+t_2) = G_{gg}(t_2)G_{ge}(t_1)\rho_{\mathrm{eq}}V_{ge}V_{\mathrm{eg}}, \tag{22b}$$

$$\rho_3(t_1+t_2) = -G_{ee}(t_2)G_{\mathrm{eg}}(t_1)V_{\mathrm{eg}}\rho_{\mathrm{eq}}V_{ge}, \tag{22c}$$

$$\rho_4(t_1+t_2) = -G_{ee}(t_2)V_{\mathrm{eg}}G_{ge}(t_1)\rho_{\mathrm{eq}}V_{ge}. \tag{22d}$$

Both fields interact with either the bra or ket for $\rho_1(t_1+t_2)$ and $\rho_2(t_1+t_2)$ and therefore these LGF constitute the roots of the hole terms in $P^{(5)}_{\mathrm{PORS}}(t,\tau,T)$. In contrast, one interaction occurs with the bra and one with the ket for the LGFs associated with the particle, $\rho_3(t_1+t_2)$ and $\rho_4(t_1+t_2)$. We note that the LGF, $\rho_i(t_1+t_2+t_3+t_4)$, depends separately on all four time arguments and not on their sum [18].

Pulses 3 and 4 are off-resonant and do not change the electronic state of the composite solute–solvent system. Therefore, only terms in which both of these interactions occur with the bra or ket (not one interaction with each) are two-photon resonant with a particular vibronic level of the electronic state populated with pulses 1 and 2. The fourth-order LGFs are obtained by operation with the material part of Eq. (10), $[\mathscr{V}\mathscr{G}(t_3)\mathscr{V}]$, on the LGFs in Eq. (22), then propagating the system for t_4 on either the ground or excited state potential energy surface. The fourth-order LGFs are

$$\rho_1(t_1+t_2+t_3+t_4) = \sum_f G_{gg}(t_4)V_{gf}G_{fg}(t_3)V_{fg}\rho_1(t_1+t_2), \tag{23a}$$

$$\rho_2(t_1+t_2+t_3+t_4) = \sum_f G_{gg}(t_4)V_{gf}G_{fg}(t_3)V_{fg}\rho_2(t_1+t_2), \tag{23b}$$

$$\rho_3(t_1+t_2+t_3+t_4) = \sum_f G_{gg}(t_4)G_{gf}(t_3)\rho_1(t_1+t_2)V_{gf}V_{fg}, \tag{23c}$$

$$\rho_4(t_1+t_2+t_3+t_4) = \sum_f G_{gg}(t_4)G_{gf}(t_3)\rho_2(t_1+t_2)V_{gf}V_{fg}, \tag{23d}$$

$$\rho_5(t_1+t_2+t_3+t_4) = \sum_f G_{ee}(t_4)V_{ef}G_{fe}(t_3)V_{fe}\rho_3(t_1+t_2), \tag{23e}$$

$$\rho_6(t_1+t_2+t_3+t_4) = \sum_f G_{ee}(t_4)V_{ef}G_{fe}(t_3)V_{fe}\rho_4(t_1+t_2), \tag{23f}$$

$$\rho_7(t_1+t_2+t_3+t_4) = \sum_f G_{ee}(t_4)G_{ef}(t_3)\rho_3(t_1+t_2)V_{ef}V_{fe}, \tag{23g}$$

$$\rho_8(t_1+t_2+t_3+t_4) = \sum_f G_{ee}(t_4)G_{ef}(t_3)\rho_4(t_1+t_2)V_{ef}V_{fe}, \tag{23h}$$

where f is an index for electronic states of the composite solute–solvent system that are off-resonant with all incident pulse frequencies. In considering the sum over f, it is important to note that the term "composite solute–solvent system" refers to the solute and the surrounding solvent molecules with which the solute interacts most significantly. The sum over f is not restricted to electronic states of the solvent.

The eight unique Liouville space pathways in the PORS response function are found by first operating on the LGFs of Eq. (23) with the material part of Eq. (10), $[\mathscr{V}\mathscr{G}(t_5)\mathscr{V}]$. The trace is then taken for terms in which the final dipole operator is projected onto the ket. These operations yield the following eight terms:

$$R_1(t_5,t_4,t_3,t_2,t_1) = \mathrm{Tr}\{\sum_{f'} V_{gf'}G_{f'g}(t_5)V_{f'g}\rho_1(t_1+t_2+t_3+t_4)\}, \quad (24a)$$

$$R_2(t_5,t_4,t_3,t_2,t_1) = \mathrm{Tr}\{\sum_{f'} V_{gf'}G_{f'g}(t_5)V_{f'g}\rho_2(t_1+t_2+t_3+t_4)\}, \quad (24b)$$

$$R_3(t_5,t_4,t_3,t_2,t_1) = \mathrm{Tr}\{\sum_{f'} V_{gf'}G_{f'g}(t_5)V_{f'g}\rho_3(t_1+t_2+t_3+t_4)\}, \quad (24c)$$

$$R_4(t_5,t_4,t_3,t_2,t_1) = \mathrm{Tr}\{\sum_{f'} V_{gf'}G_{f'g}(t_5)V_{f'g}\rho_4(t_1+t_2+t_3+t_4)\}, \quad (24d)$$

$$R_5(t_5,t_4,t_3,t_2,t_1) = \mathrm{Tr}\{\sum_{f'} V_{ef'}G_{f'e}(t_5)V_{f'e}\rho_5(t_1+t_2+t_3+t_4)\}, \quad (24e)$$

$$R_6(t_5,t_4,t_3,t_2,t_1) = \mathrm{Tr}\{\sum_{f'} V_{ef'}G_{f'e}(t_5)V_{f'e}\rho_6(t_1+t_2+t_3+t_4)\}, \quad (24f)$$

$$R_7(t_5,t_4,t_3,t_2,t_1) = \mathrm{Tr}\{\sum_{f'} V_{ef'}G_{f'e}(t_5)V_{f'e}\rho_7(t_1+t_2+t_3+t_4)\}, \quad (24g)$$

$$R_8(t_5,t_4,t_3,t_2,t_1) = \mathrm{Tr}\{\sum_{f'} V_{ef'}G_{f'e}(t_5)V_{f'e}\rho_8(t_1+t_2+t_3+t_4)\}, \quad (24h)$$

where f' is an index for electronic states of the composite solute–solvent system that are off-resonant with respect to all incident pulse frequencies. Again, as discussed in the context of Eq. (23), the sum over f' is not restricted to electronic states of the solvent.

The double-sided Feynman diagrams corresponding to each of these terms are presented in Fig. 7 [18]. The hole pathways R_1–R_4 have positive signs as a result of an even number of interactions with the bra, whereas the particle pathways R_5–R_8 have an odd number of interactions with the bra and negative signs. Thus, the signals corresponding to the particle and hole are 180° out-of-phase. In terms of the model presented above, the $\Phi_j^g(\tau,T)$, and $\Phi_j^e(\tau,T)$ terms of Eq. (20) convolute the spectrum of the resonant pulse

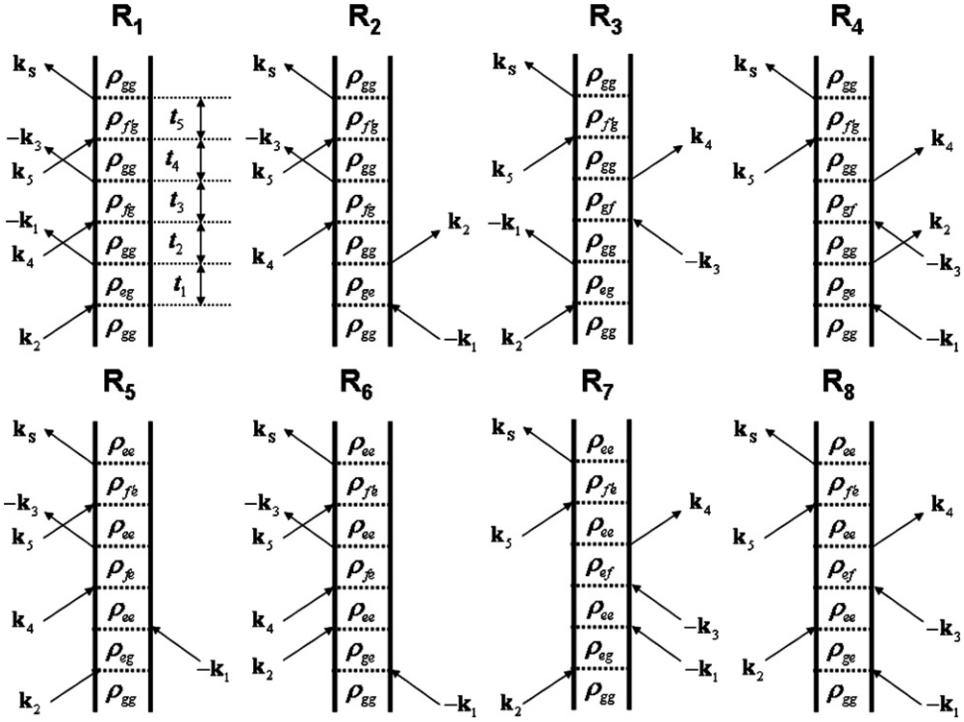

Fig. 7. Double-sided Feynman diagrams corresponding to terms given in Eq. (24). Pathways $R_1 - R_4$ and $R_5 - R_8$ represent ground and excited state contributions, respectively. The hole and particle terms have even and odd numbers of interactions with the bra and therefore have opposite signs. Pathways $R_1 - R_4$ and $R_5 - R_8$ give rise to signals that are 180 out-of-phase.

pair, $E_1\&E_2$ (i.e., $I(\omega_1' - \omega_1)$ of Eq. (9)), with sums of the R_1–R_4 and R_5–R_8 terms, respectively.

5. Conclusion

We have presented a formalism in which the PORS experiment is treated as a sequential process. The source of the signal is expressed as a three-time nonequilibrium correlation function that resembles the third-order equilibrium polarizability susceptibility, which is a two-time correlation function. The resulting numerical model has been used to illustrate the two primary mechanisms of PORS signal generation: structural relaxation-induced resonance and dephasing-induced resonance. Comparison of model calculations with experiments suggests that structural relaxation-induced resonance is the primary origin of the PORS signals observed for the C153-solvent systems. Terms in the PORS correlation function associated with ground (hole) and excited (particle) state populations are shown to have opposite signs. The amount of interference between hole and particle terms is represented by the overlap of semiclassical nuclear wavepackets in coordinate space.

The eight dominant terms in the PORS response function are presented as double-sided Feynman diagrams in Section 4. The hole (particle) diagrams are shown to involve an even (odd) number of interactions with the bra. Thus, the hole and particle terms have opposite signs and their respective signals are 180° out-of-phase. The resulting interferences are similar in origin to the dephasing-induced resonances observed in electronically resonant coherent Raman spectroscopies (CRS) [32–34]. In CRS, terms involving ground and excited state populations are also 180° out-of-phase. Similar fifth-order spectroscopies such as the FSRS technique [37] and RaPTORS [21,28,29] should also exhibit effects of interfering terms and may be described with a similar approach to that presented here.

This formalism has now been used to interpret the PORS signals associated with an intermolecular charge transfer reaction [26,27]. This interpretation has established the contribution of solvent dynamics to the measured reaction rates. We suggest that the information content of the time-evolving (in T) spectral densities transcends the previous "time-integrated" descriptions (e.g., that were appropriate for time-dependent fluorescence Stokes shift measurements). These reaction time-dependent spectral densities will be particularly important in cases in which the nonadiabatic limit of charge transfer does not hold, where solvation and reaction dynamics occur on the same time-scale.

Acknowledgements

We thank the National Science Foundation (CHE 0317009) for support. N.F.S. acknowledges the John S. Guggenheim Foundation for a Fellowship.

Appendix A. Heterodyne detection

Expression of the heterodyned signal in PORS, as it is implemented in our experiments [25,30], should begin with recognition that interference between the local oscillator (LO) and signal pulses is accomplished by varying the optical path length of the LO in a glass cover slip, which means that the group delay imparted to the LO is more important for heterodyne detection than the change in its phase velocity (~25× more important for BK7 glass). We make this distinction because variation of the LO phase, ϕ^0_{LO}, and envelope delay, $\bar{\tau}_{\mathrm{LO}}$, are experimentally distinguishable [44] and alternative methods of heterodyne detection allow for cycling of the LO phase with a fixed envelope delay [45,46]. The envelope-delayed interference signal may be expressed by writing the LO field as

$$E_{\mathrm{LO}}(\mathbf{k}_{\mathrm{LO}}, t) = \epsilon_{\mathrm{LO}}(t - \bar{\tau}_{\mathrm{LO}}) \exp[\mathrm{i}\mathbf{k}_{\mathrm{LO}}\mathbf{r} - \mathrm{i}\bar{\omega}_{\mathrm{LO}}(t - \bar{\tau}_{\mathrm{LO}}) - \mathrm{i}\phi^0_{\mathrm{LO}}] \tag{A.1}$$

and defining the fields for all other pulses with Eq. (7). These definitions are appropriate for the experiments because the envelope delays and phases of pulses 1–5 (and the signal) are fixed for a measurement of the signal at a single pair of delays, (T, τ) [25,30]. Eq. (A.1) suggests that the phase of the LO may be effectively varied with respect to a fixed reference field (i.e., the signal) by changing the delay, $\bar{\tau}_{\mathrm{LO}}$. For example, a difference in the delay of half the optical period, $\Delta\bar{\tau}_{\mathrm{LO}} = 1/\bar{\omega}_{\mathrm{LO}}$, approximates a phase shift of $\Delta\phi^0_{\mathrm{LO}} = \pi$ with respect to a fixed reference field provided that the pulse duration is long compared to a single optical cycle.

The total detected signal intensity is a superposition of the LO and signal fields and may be expressed as

$$I_{\mathrm{tot}}(\tau, T) = \int_{-\infty}^{\infty} \mathrm{d}t |E_{\mathrm{LO}}(t) + E^{(5)}_{\mathrm{PORS}}(t, \tau, T)|^2. \tag{A.2}$$

The phase-sensitive cross term in Eq. (A.2) is given by

$$I_{\mathrm{het}}(\tau, T; \Delta\phi_{\mathrm{het}}) = 2\int_{-\infty}^{\infty} \mathrm{d}t E_{\mathrm{LO}}(t) E^{(5)}_{\mathrm{PORS}}(t, \tau, T) \cos(\Delta\phi_{\mathrm{het}}), \tag{A.3}$$

where $\Delta\phi_{\mathrm{het}} = \phi^0_S - \phi^0_{\mathrm{LO}} + \bar{\omega}_{\mathrm{LO}}\bar{\tau}_{\mathrm{LO}}$. Eq. (A.3) is further decomposed into the real (absorptive) and imaginary (dispersive) parts of $P^{(5)}_{\mathrm{PORS}}(t, \tau, T)$:

$$\begin{aligned} I_{\mathrm{het}}(\tau, T; \Delta\phi_{\mathrm{het}}) = \frac{4\pi l \bar{\omega}_t}{n(\bar{\omega}_t)c} \int_{-\infty}^{\infty} \mathrm{d}t E_{\mathrm{LO}}(t) \\ \times [Re\{P^{(5)}_{\mathrm{PORS}}(t, \tau, T)\} \sin(\Delta\phi_{\mathrm{het}}) \\ + Im\{P^{(5)}_{\mathrm{PORS}}(t, \tau, T)\} \cos(\Delta\phi_{\mathrm{het}})]. \end{aligned} \tag{A.4}$$

The heterodyne-detected phase, $\Delta\phi_{\mathrm{het}}$, is determined with an experimental calibration procedure [25,30].

The PORS experiment selectively measures of the dispersive part of the signal with a method analogous to phase cycling in NMR [47] and the elimination of "homodyne" signals in optical Kerr effect spectroscopy [48]. The signal

is isolated by measuring $I_{\mathrm{tot}}(\tau, T; \Delta\phi_{\mathrm{het}})$ at two phase angles, $\Delta\phi_{\mathrm{het}} = \pi/2$ and $\Delta\phi_{\mathrm{het}} = 3\pi/2$, and taking their difference:

$$S_{\mathrm{PORS}}(\tau, T) \equiv I_{\mathrm{tot}}(\tau, T; \Delta\phi_{\mathrm{het}} = \pi/2) - I_{\mathrm{tot}}(\tau, T; \Delta\phi_{\mathrm{het}} = 3\pi/2). \quad (A.5)$$

This procedure eliminates the homodyned terms in Eq. (A.2), $|E_{\mathrm{LO}}(t)|^2 + |E^{(5)}_{\mathrm{PORS}}(t, \tau, T)|^2$, that are insensitive to the phase of the local oscillator. Furthermore, four phase-insensitive third-order "pump–probe" signals, which are emitted into the same phase-matched direction as the PORS signal, are also eliminated by Eq. (A.5). These signals have the wavevectors $-\mathbf{k_1} + \mathbf{k_2} + \mathbf{k}_{\mathrm{LO}}$, $-\mathbf{k_3} + \mathbf{k_3} + \mathbf{k}_{\mathrm{LO}}$, $-\mathbf{k_4} + \mathbf{k_4} + \mathbf{k}_{\mathrm{LO}}$ and $-\mathbf{k_5} + \mathbf{k_5} + \mathbf{k}_{\mathrm{LO}}$.

The importance of third-order cascaded contributions should be evaluated for PORS as these signals are known to affect and even dominate fifth-order off-resonant Raman spectroscopy of neat liquids [49]. For the boxcars geometry used in our experiments, the dispersive components of third-order cascaded signals are 90° out-of-phase from the PORS signal and are not amplified by the LO. Our experiments show that there is virtually no signal at the phase-angle in quadrature to the (dispersive) PORS signal for the C153-solvent systems [25,30]. Heterodyned detection was critical for measuring the pure fifth-order off-resonant Raman signals amid a strong background of third-order cascades, which (as in PORS) are 90° out-of-phase with the fifth-order signal of interest [50]. It is also important to note that the ratio of the cascaded response to the fifth-order PORS signal amplitude is linear in concentration [51–53]. Therefore, signal contamination by cascades should be significantly reduced in fifth-order experiments that study solutes (or solute–solvent systems such as PORS) compared to those that study pure liquids. Nonetheless, it is not clear that cascades will be inherently negligible for all applications of the PORS technique and this issue should be addressed on a case by case basis.

Appendix B. PORS and linear response theory

In this appendix, we show how the approximation of linear response is used to write the *nonequilibrium* correlation function in Eq. (20). To clarify the assumptions involved, we first show that this relation is valid for the third-order *equilibrium* polarizability susceptibility (Eq. (12)).

Expanded in a basis of discrete levels for a single harmonic mode, the third-order polarizability susceptibility is expressed as

$$\chi(t) = \frac{-\mathrm{i}}{\hbar}\sum_{a,c}[\langle\alpha_{ac}(t)\alpha_{ca}(0)\rho_{aa}\rangle - \langle\alpha_{ca}(t)\alpha_{ac}(0)\rho_{cc}\rangle] \times \exp(-\mathrm{i}\omega_{ca}t), \quad (B.1)$$

where ρ_{aa} is the equilibrium population for level a. Under the detailed balance condition, the population difference for levels a and c is given by

$$\rho_{aa} - \rho_{cc} = \left[1 - \exp\left(-\frac{\hbar\omega_{ca}}{kT}\right)\right]\rho_{aa}, \quad (B.2)$$

which allows Eq. (B.1) to be rewritten as

$$\chi(t) = \frac{-\mathrm{i}}{\hbar}\sum_{a,c}\left[1 - \exp\left(-\frac{\hbar\omega_{ca}}{kT}\right)\right]\langle\alpha_{ac}(t)\alpha_{ca}(0)\rho_{aa}\rangle \times \exp(-\mathrm{i}\omega_{ca}t). \quad (B.3)$$

In the limit of homogeneous vibrational dephasing, Eq. (B.3) becomes

$$\chi(t) = \frac{-\mathrm{i}}{\hbar}\sum_{a,c}\left[1 - \exp\left(-\frac{\hbar\omega_{ca}}{kT}\right)\right]\langle|\alpha_{ac}(0)|^2\rho_{aa}\rangle \times \exp(-\mathrm{i}\omega_{ca}t - \Gamma_{ca}t). \quad (B.4)$$

The detailed balance condition (Eq. (B.2)) clearly holds for a system at thermal equilibrium. However, Eq. (20) involves projecting the polarizabilities onto the nonequilibrium wavepacket, $D^m_j(q_j, T)$. The fundamental assumption of Eq. (20) is then expressed as

$$D^m_{aa}(q_j, T) - D^m_{cc}(q_j, T) = \left[1 - \exp\left(-\frac{\hbar\omega_{ca}}{kT}\right)\right]D^m_{aa}(q_j, T), \quad (B.5)$$

where $D^m_{aa}(q_j, T)$ describes the evolution of a harmonic nuclear mode j in the discrete level a during the pulse delay T. Eq. (B.5) holds in the approximation of linear response. This means that the displacement of the nuclear mode from its equilibrium position is small and indistinguishable from a spontaneous fluctuation at equilibrium (i.e., the fluctuation–dissipation theorem). Overtone excitations are neglected in Eq. (20) and $D^m_{aa}(q_j, T) - D^m_{cc}(q_j, T)$ is written as $D^m_j(q_j, T)$ with the index of its quantum state omitted. In general, it may be useful to consider overtone transitions for systems with large reorganization energies because such systems should exhibit significant Huang-Rhys factors for overtones.

The low frequency modes considered here are taken to be poorly resolved due to spectral broadening. Therefore, we use a correlation function approach rather than a sum over quantum states formulation. The coordinate dependence of the PORS response can be understood by expanding the polarizability $\alpha_j(q_j)$ of Eq. (20) as

$$\alpha[q^m_j(T)] = \alpha[q^m_j(T)] + \sum_j \alpha'[q^m_j(T)]q^m_j(T) + \cdots, \quad (B.6)$$

where

$$\alpha'[q^m_j(T)] = \left(\frac{\partial\alpha}{\partial q_j}\right)_{q^m_j(T)}. \quad (B.7)$$

The coordinate $q^m_j(T)$ is defined by Eq. (16). The derivative of the polarizability in Eq. (B.7) is evaluated at the position of the coordinate, q_j, in state m at time T. To first order, the leading term of Eq. (B.6) does not contribute to the PORS correlation function,

$$\Phi_j^m(\tau,T)=\frac{i|\mu_{eg}|^2}{\hbar^5}\langle[\alpha_j(0),\alpha_j(\tau)]D_j^m(T)\rangle, \quad (B.8)$$

as it causes the commutator to vanish. By inserting the expansion of Eq. (B.6) and keeping the leading term we obtain

$$\Phi_j^m(\tau,T)=\frac{i|\mu_{eg}|^2}{\hbar^5}|\alpha'[q_j^m(T)]|^2\langle[q_j(0),q_j(\tau)]D_j^m(T)\rangle. \quad (B.9)$$

The dephasing rates, Γ_j^m, (Eq. (20)) should be independent of the value of T under the approximation of linear response. In other words, Γ_j^m, must be coordinate independent within the q_j space traversed by $D_j^m(q_j,T)$ because thermal fluctuations of the system are uniform within this q_j space. Our experimental data show that Γ_j^m evolves in T and therefore suggests that the approximation of linear response does not hold for the Coumarin 153-acetonitrile system [25,30]. Blank and Underwood have reached a similar conclusion with the RaPTORS technique for Coumarin 102 in acetonitrile [21].

Appendix C. Solvation time-scales and PORS linewidths

Comparison of Eq. (8.63b) of Ref. [18] and Eq. (B.8) above suggests that the imaginary part of the energy gap correlation function, $C_j''(\tau)$, and the Raman response measured with PORS are related by

$$C_j''(\tau)\equiv-\frac{\hbar^5}{2|\alpha_j'|^2|\mu_{eg}|^2}\Phi_j^g(\tau,T=0). \quad (C.1)$$

The PORS correlation function associated with the ground state, $\Phi_j^g(\tau,T=0)$, at $T=0$ is referenced in Eq. (C.1) because the system is at equilibrium before its interaction with the electronically resonant laser pulse pair, $E_1\&E_2$, whereas Eq. (8.63b) of Ref. [18] projects position operators onto the equilibrium density operator of the system. The solvation correlation function used in Section 3.5, $M_j(t)$, is expressed as [18]

$$M_j(T)=\frac{1}{\pi\Delta^2}\int_0^\infty d\omega C_j''(\omega)\coth(\beta\hbar\omega/2)\cos(\omega T), \quad (C.2)$$

where

$$C_j''(\omega)\equiv 2\int_0^\infty d\tau C_j''(\tau)\sin(\omega\tau). \quad (C.3)$$

Thus, the relationship between the Raman response in τ (Eq. (C.1)) and the solvation dynamics in T (Eq. (C.2)) is defined by linear response theory.

Our numerical calculations have taken the time evolution of $M_j(T)$ to be overdamped and independent from the lineshape of the Raman spectrum associated with the delay, τ. It is important to account for underdamped nuclear coherences in T for certain systems because they can give rise to recurrences of the signal phase [54]. However, we measure no amplitude or phase recurrences in T for the C153 systems considered here [25,30] or for a recent application of PORS to a pyridinium iodide complex [26,27]. We therefore model the data with an overdamped correlation function in T as this provides better agreement with experimental observations. These data suggest that a theory not based on the linear response approximation may be more appropriate as a description of dipole solvation in liquids. Further studies with broadband electronically resonant pulses capable of exciting underdamped nuclear coherences in T will be useful for further understanding this issue.

References

[1] L. Lehr, M.T. Zanni, C. Frischkorn, R. Weinkauf, D.M. Neumark, Science 284 (1999) 635.
[2] V.H. Vilchiz, J.A. Kloepfer, A.C. Germaine, V.A. Lenchenkov, S.E. Bradforth, J. Phys. Chem. A 105 (2001) 1711.
[3] E.R. Barthel, I.B. Martini, E. Keszei, B.J. Schwartz, J. Chem. Phys. 118 (2003) 5916.
[4] W. Jarzeba, G.C. Walker, A.E. Johnson, M.E. Kahlow, P.F. Barbara, J. Chem. Phys. 90 (1989) 151.
[5] M.A. Kahlow, W. Jarzeba, T.J. Kang, P.F. Barbara, J. Chem. Phys. 90 (1989) 151.
[6] S.J. Rosenthal, X. Xie, M. Du, G.R. Fleming, J. Chem. Phys. 95 (1991) 4715.
[7] R. Jiminez, G.R. Fleming, P.V. Kumar, M. Maroncelli, Nature (London) 369 (1994) 471.
[8] L. Reynolds, J.A. Gardecki, J.V. Frankland, M.L. Horng, M. Maroncelli, J. Phys. Chem. 100 (1996) 10337.
[9] C.H. Brito-Cruz, R.L. Fork, W.H. Knox, C.V. Shank, Chem. Phys. Lett. 132 (1986) 341.
[10] T.J. Kang, Y. Jongwan, M. Berg, J. Chem. Phys. 94 (1991) 2413.
[11] H. Murakami, S. Kinoshita, Y. Hirata, T. Okada, N. Mataga, J. Chem. Phys. 97 (1992) 7881.
[12] W.P. de Boeij, M.S. Pshenichnikov, D.A. Wiersma, Annu. Rev. Phys. Chem. 49 (1998) 99.
[13] M.J. Lang, X.J. Jordanides, X. Song, G.R. Fleming, J. Chem. Phys. 110 (1999) 5884.
[14] T.S. Yang, P. Vohringer, N.F. Scherer, J. Chem. Phys. 103 (1995) 8346.
[15] L.D. Book, N.F. Scherer, J. Chem. Phys. 111 (1999) 792.
[16] D.M. Jonas, Annu. Rev. Phys. Chem. 54 (2003) 425.
[17] R. Kubo, Adv. Chem. Phys. 15 (1969) 101.
[18] S. Mukamel, Principles of Nonlinear Optical Spectroscopy, Oxford University Press, New York, Oxford, 1995.
[19] K. Kwac, M. Cho, J. Chem. Phys. 120 (2004) 1477.
[20] T. Steinel, J.B. Asbury, S.A. Corcelli, C.P. Lawrence, J.L. Skinner, M.D. Fayer, Chem. Phys. Lett. 386 (2004) 295.
[21] D.F. Underwood, D.A. Blank, J. Phys. Chem. A 109 (2005) 3295.
[22] J. Bredenbeck, J. Helbing, P. Hamm, Phys. Rev. Lett. 95 (2005) 083201.
[23] P. Hamm, J. Chem. Phys. 124 (2006) 124506.
[24] S. Park, J. Kim, N.F. Scherer, Ultrafast Phenomena XIV 79 (2005) 557.
[25] S. Park, A.M. Moran, J. Kim, N.F. Scherer, in preparation.
[26] A.M. Moran, R.A. Nome, S. Park, N.F. Scherer, J. Chem. Phys. (2007) in press.
[27] A.M. Moran, R.A. Nome, N.F. Scherer, Phys. Rev. Lett., 2007, submitted for publication.
[28] D.F. Underwood, D.A. Blank, J. Phys. Chem. A 107 (2003) 956.
[29] S.J. Schmidtke, D.F. Underwood, D.A. Blank, J. Phys. Chem. A 109 (2005) 7033.
[30] S. Park, One- and two-dimensional polarizability response spectroscopy: studies of ultrafast solvent dynamics in solvation, Ph.D. Thesis, The University of Chicago, 2006.
[31] Y.J. Yan, L.E. Fried, S. Mukamel, J. Phys. Chem. 93 (1989) 8149.

[32] A.R. Bogdan, M.W. Downer, N. Bloembergen, Phys. Rev. A 24 (1981) 623.
[33] J.R. Andrews, R.M. Hochstrasser, Chem. Phys. Lett. 82 (1981) 381.
[34] L.J. Rothberg, N. Bloembergen, Phys. Rev. A 30 (1984) 820.
[35] R. Venkatramani, S. Mukamel, J. Phys. Chem. B 109 (2005) 8132.
[36] D.W. McCamant, P. Kukura, S. Yoon, R.A. Mathies, Rev. Sci. Instrum. 75 (2004) 4971.
[37] P. Kukura, D.W. McCamant, S. Yoon, D.B. Wandschneider, R.A. Mathies, Science 310 (2005) 1006.
[38] D. McMorrow, W.T. Lotshaw, Chem. Phys. Lett. 174 (1990) 85.
[39] S. Park, B.N. Flanders, X. Shang, R.A. Westervelt, J. Kim, N.F. Scherer, J. Chem. Phys. 118 (2003) 3917.
[40] Y.J. Chang, E.W.J. Castner, J. Phys. Chem. 100 (1996) 3330.
[41] M.L. Horng, J.A. Gardecki, M. Maroncelli, J. Phys. Chem. 99 (1995) 17311.
[42] F. Cichos, R. Brown, P.A. Bopp, J. Chem. Phys. 114 (2001) 6834.
[43] F. Ingrosso, B. Ladanyi, M.D. Menucci, M.D. Elola, J. Tomasi, J. Phys. Chem. B 109 (2005) 3353.
[44] A.W. Albrecht, J.D. Hybl, S.M. Gallagher, D.M. Jonas, J. Chem. Phys. 111 (1999) 10934.
[45] J.C. Vaughn, T. Feurer, K.A. Nelson, J. Opt. Soc. Am. B 19 (2002) 2489.
[46] P. Tian, D. Keusters, Y. Suzaki, W.S. Warren, Science 300 (2003) 1553.
[47] R.R. Ernst, G. Bodenhausen, A. Wokaun, Principles of Nuclear Magnetic Resonance in One and Two Dimensions, Oxford University Press, New York, 1987.
[48] D. McMorrow, W.T. Lotshaw, G.A. Kenney-Wallace, IEEE J. Quantum Electron. 24 (1988) 443.
[49] D.A. Blank, L.J. Kaufman, G.R. Fleming, J. Chem. Phys. 111 (1999) 3105.
[50] K.J. Kubarych, C.J. Milne, S. Lin, V. Astinov, R.J.D. Miller, J. Chem. Phys. 116 (2002) 2016.
[51] J.E. Ivanecky, J.C. Wright, Chem. Phys. Lett. 206 (1993) 437.
[52] J.C. Kirkwood, A.C. Albrecht, J. Raman Spectrosc. 31 (2000) 107.
[53] E.C. Fulmer, F. Ding, M.T. Zanni, J. Chem. Phys. 122 (2005) 034302.
[54] P. Kukura, R. Frontiera, R.A. Mathies, Phys. Rev. Lett. 96 (2006) 238303.